6400 *Biochemistry* **2010,** *49,* 6400–6410
DOI: 10.1021/bi1004206

BIOCHEMISTRY
including biophysical chemistry & molecular biology
Article

Substrate-Induced Closing of the Active Site Revealed by the Crystal Structure of Pantothenate Synthetase from *Staphylococcus aureus*[†]

Atsuko Satoh,[‡] Saki Konishi,[‡] Haruka Tamura,[‡] Hannah G. Stickland,[§] Heather M. Whitney,[§] Alison G. Smith,[§] Hiroyoshi Matsumura,*[,‡,∥] and Tsuyoshi Inoue[‡,∥]

[‡]*Department of Applied Chemistry, Graduate School of Engineering, Osaka University, 2-1 Yamadaoka, Suita, Osaka 565-0871, Japan,* [§]*Department of Plant Sciences, University of Cambridge, Downing Street, Cambridge CB2 3EA, United Kingdom, and* [∥]*CREST, JST, 2-1 Yamadaoka, Suita, Osaka 565-0871, Japan*

Received March 21, 2010; Revised Manuscript Received June 20, 2010

ABSTRACT: Pantothenate synthetase (PS, EC 6.3.2.1) is the last enzyme in the pantothenate biosynthesis pathway, a metabolic pathway identified as a potential target for new antimicrobials. PS catalyzes the ATP-dependent condensation of pantoate and β-alanine to form pantothenate. Here we report the overexpression, purification, enzyme assay, and tertiary structure of PS from *Staphylococcus aureus*. PS activity was experimentally confirmed, indicating a k_{cat} value comparable to those of enzymes from other organisms. The structures of the apoenzyme and the reaction intermediate (pantoyl adenylate; PA) complex were determined by X-ray crystallography to resolutions of 2.5 and 1.85 Å, respectively. Structural analysis indicated that the apoenzyme adopts an open and relatively mobile structure, while the complex structure is closed and entirely rigid. Structural comparison of the apoenzyme and the complex revealed how *S. aureus* PS undergoes open/close conformational change, and also determined the key interactions with the adenine ring of PA for a hinge bending domain closure. In the complex structure, PA and acetate are bound in the active site. We suggest that the acetate mimics the substrate β-alanine. Therefore, the complex structure seems to represent a catalytic state poised for in-line nucleophilic attack on PA. These data also offer an alternative strategy for designing novel compounds that selectively inhibit PS activity.

Pantothenate (vitamin B_5) is the precursor of the 4′-phosphopantetheine moiety of coenzyme A (CoA) and acyl carrier protein (ACP), enzyme cofactors essential for key metabolic and energy-yielding reactions in living cells (*1*, *2*), including fatty acid synthesis and oxidization, transcription, cell signaling, and the biosynthesis of polyketides and nonribosomal peptides (*3*−*7*). Pantothenate is synthesized *de novo* in bacteria, yeast, and plants (*8*), but mammals must obtain pantothenate in their diet, so the enzymes of the pathway are potential targets for antimicrobial agents. Studies in immunocompromised and immunocompetent mice have demonstrated that a *Mycobacterium tuberculosis* mutant defective in pantothenate biosynthesis (*9*) is attenuated in its ability to cause disease, implicating the need for a functional pantothenate biosynthetic pathway in the virulence of *M. tuberculosis*. Proteomic analysis showed that an enzyme (Sar2676) annotated as pantothenate synthetase (PS)[1] in the pathway is upregulated in methicillin-resistant *Staphylococcus aureus* (MRSA), compared with a methicillin-sensitive strain of *S. aureus* (*10*). Thus, biochemical and structural studies of this pathway offer potential for the discovery of a drug that acts against pathogenic microbes.

The pantothenate biosynthesis pathway is best characterized in *Escherichia coli*, and it comprises four enzymes encoded by the *panB*, *panC*, *panD*, and *panE* genes (*11*, *12*). The *panC* gene encodes a PS (EC 6.3.2.1), an adenosine triphosphate (ATP) dependent enzyme that catalyzes the condensation of D-pantoate and β-alanine to form pantothenate (*13*). Native PS has been purified from many organisms (*13*), and in addition recombinant PS has been purified and partly characterized from bacteria (*E. coli* and *M. tuberculosis*), fungi (*Fusarium oxysporum* and *Saccharomyces cerevisiae*), and higher plants (*Lotus japonicus* and *Arabidopsis thaliana*) (*14*−*16*). In all cases *E. coli* and *M. tuberculosis* PS enzymes appear to be functional homodimers with a subunit molecular mass of about 30−35 kDa.

Previous kinetic analysis showed that PS utilizes an ordered bi-uni uni-bi ping-pong kinetic mechanism, with ATP binding first, followed by D-pantoate binding, release of PP_i, and binding of β-alanine (*14*). The enzyme-catalyzed reaction is believed to proceed in two steps: the formation of an enzyme-bound intermediate, pantoyl adenylate (PA), from ATP and pantoate, followed by nucleophilic attack on the intermediate by β-alanine to form pantothenate and AMP (Scheme 1).

The crystal structures of both *E. coli* and *M. tuberculosis* PS enzymes have been reported (*17*−*24*). Several complexes and apo structures of the *M. tuberculosis* enzyme are available, and the apo structure and the pantoate complex of the N-terminal domain structure are available for *E. coli* PS. In addition,

[†]This work was supported by the Knowledge Cluster Initiative promoted by the Ministry of Education, Culture, Sports, Science, and Technology, the UK Biotechnology and Biological Sciences Research Council, and the Japan Society for the Promotion of Science. H.T. was a recipient of a Research Fellowship from the Japan Society for the Promotion of Science for Young Scientists.

*To whom correspondence should be addressed. Tel: 816-6879-7410. Fax: 816-6879-7409. E-mail: matsumura@chem.eng.osaka-u.ac.jp.

[1]Abbreviations: PS, pantothenate synthetase; PA, pantoyl adenylate; ATP, adenosine 5′-triphosphate; AMP, adenosine 5′-monophosphate; *S. aureus*, *Staphylococcus aureus*; *E. coli*, *Escherichia coli*; *M. tuberculosis*, *Mycobacterium tuberculosis*; *T. thermophilus* HB8, *Thermus thermophilus* HB8; *T. maritima*, *Thermotoga maritima*; *B. melitensis*, *Brucella melitensis*; NADH, reduced β-nicotinamide adenine dinucleotide; SDS−PAGE, sodium dodecyl sulfate−polyacrylamide gel electrophoresis; NCS, non-crystallographic symmetry; ASU, asymmetric unit.

 Published on Web 06/22/2010

Scheme 1: Reaction Mechanism Catalyzed by PS

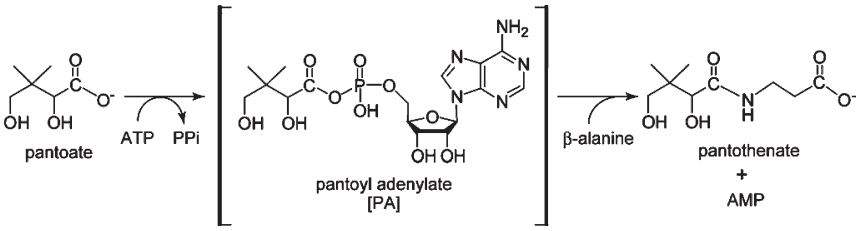

structural genomics projects recently determined the apo structures of proteins annotated as PS of *Thermus thermophilus HB8* (PDB entries 1UFV and 1V8F) and *Thermotoga maritima* (PDB entry 2EJC) and the ATP complex structure of a protein annotated as PS of *Brucella melitensis* (PDB entry 3INN). In general, the PS protomer can be divided into two domains (N- and C-terminal domains), with the active site located at the interface of these domains. The current literature suggests that *E. coli* PS is expected to utilize the hinge movement of the C-terminal domain to open and close the active site during the enzymatic reaction (*17*), because the catalytically essential residues are spatially separated into two domains in the apo structure of the *E. coli* enzyme. However, this remains an assumption, due to the absence of the ternary structure of the full-length *E. coli* PS. Moreover, *M. tuberculosis* PS, whose structures are available for both the apoenzyme and the PA complex, exhibits no large conformational change upon substrate binding (*18*, *19*). The molecular mechanism of the hinge bending domain closure in PS thus remains unknown.

Here we describe overexpression, purification, enzyme assay, and crystal structures of the apoenzyme and the PA complex of *S. aureus* PS. Structural analysis demonstrated that *S. aureus* PS undergoes open/close conformational change, giving the first direct evidence of a hinge bending domain closure in PS. The key interactions to trigger the hinge movement are found between the hinge region and the adenine ring of PA. The structure also represents a catalytic state poised for in-line nucleophilic attack in the PS reaction. These results are expected to be applicable for the design of compounds that selectively inhibit PS activity.

MATERIALS AND METHODS

Construction of the Plasmid. The *S. aureus panC* gene (GenBank accession number YP_501370.1) was amplified by PCR from genomic DNA of *S. aureus* strain NCTC8325 (forward primer, 5′-ATG ACT AAG CTG TTA CTA CGG-3′; reverse primer, 5′-TTA TTC AGC TCC AAT TAT TAT AT-3′). The PCR products were ligated into pGEMT Easy vector using T4 DNA ligase (Promega), and the resulting plasmid pGEM-*panC* was transformed into *E. coli* DH5α. The insert DNA was sequenced to confirm that it was identical to the *panC* gene from strain NCTC8325. For construction of the expression vector, the *panC* gene was amplified by PCR using pGEM-*panC* as a template (forward primer, 5′-TAT ATA CAT ATG ACT AAG CTG ATT ACT ACG-3′; reverse primer, 5′-TAT ATA GGA TCC TTA TTC AGC TCC AAT TAT TAT ATT ATC-3′) to generate *Nde*I and *Bam*HI restriction sites (underlined). After restriction enzyme digestion of the vector and PCR product with *Nde*I and *Bam*HI, the resulting *panC* fragment was then ligated into pET16b (Novagen), generating a construct to express the *panC* gene with an N-terminal His_6 tag. However, the construct was transformed into *E. coli* strain BL21(DE3) (Invitrogen), the expression level of soluble PS was very low. The DNA encoding *panC* gene was further cloned into a pCold TF (TaKaRa) expression vector. The *panC* gene was amplified by PCR from a template of pET16b-*panC* (forward primer, 5′-TAT ATA CAT ATG ACT AAG CTG ATT ACT ACG-3′; reverse primer, 5′-TAT ATA GGA TCC TTA TTC AGC TCC AAT TA-3′) to generate *Nde*I and *Bam*HI restriction sites (underlined). After restriction enzyme digestion of the amplified DNA, the resulting *panC* fragment was then ligated into the pCold TF vector, generating a construct to express the *panC* gene with an N-terminal His_6 and trigger factor tag, cleavable by proteases (HRV 3C protease, thrombin, and factor Xa). The construct was confirmed by DNA sequencing and then transformed into *E. coli* DH5α cells (Invitrogen). The resulting plasmids were spin-column purified and transformed into BL21(DE3) competent cells for protein overexpression. The expression level of soluble PS was much improved, confirmed by SDS−PAGE; therefore, we decided to use this system for subsequent crystallization and characterization experiments.

Expression and Purification. The transformed BL21(DE3) cells containing *S. aureus panC* cloned into pCold TF were grown in Luria broth medium containing 100 μg/mL ampicillin at 37 °C to an OD_{600} of 0.6−1.0 and then induced with 1 mM isopropyl β-D-thiogalactopyranoside overnight at 15 °C. The harvested cell pellets from 2 L of bacterial culture were resuspended with 60 mL of buffer (2 mM Tris-HCl, pH 8.0, 5 mM NaCl, 1 mM imidazole) and lysed by sonication. Cell lysate was centrifuged at 6300*g* for 30 min at 4 °C, and the supernatant was loaded onto a Ni^{2+}-charged HiTrap chelating column (GE Healthcare), which was preequilibrated with 20 mM Tris-HCl, pH 8.0, 500 mM NaCl, and 10 mM imidazole. The column was washed with 15 column volumes of the same buffer and eluted with a linear gradient of imidazole from 10 to 500 mM in 20 mM Tris-HCl, pH 8.0, and 500 mM NaCl. The fractions containing PS protein were pooled and concentrated, and the protein was further purified on a Superdex 200 column (GE Healthcare) equilibrated with 20 mM Tris-HCl, pH 8.0, 300 mM NaCl, and 5 mM DTT. The fractions containing PS protein were pooled and concentrated, and the N-terminal His_6 and trigger factor tag was digested with HRV 3C protease (Novagen) overnight at 4 °C in a solution containing 50 mM Tris-HCl, pH 7.5, and 150 mM NaCl. After the solution was brought to a final concentration of 40% saturated $(NH_4)_2SO_4$, the sample was loaded onto a HiTrap butyl column (GE Healthcare) equilibrated with 20 mM Tris-HCl, pH 8.0, 5 mM DTT, and saturated 40% $(NH_4)_2SO_4$ to separate the digested protein from the undigested protein, cleaved N-terminal tag, and protease. The column was washed with 15 column volumes of the same buffer and eluted with a linear gradient of saturated $(NH_4)_2SO_4$ concentration from 40% to 0% in 20 mM Tris-HCl, pH 8.0, and 5 mM DTT. The fractions containing PS protein were pooled and concentrated. The protein was further purified on a Superdex 200 column equilibrated with 20 mM Tris-HCl, pH 8.0, 300 mM NaCl, and 5 mM DTT. The eluted fractions were collected and analyzed by SDS−PAGE.

Protein concentrations were determined using a Bio-Rad protein assay kit with bovine serum albumin as the standard.

Coupled Assay of PS Activity. PS activity was measured spectrophotometrically in a coupled reaction as described by Miyatake et al. (*13*) and modified in ref *15*; AMP, generated by the PS reaction, was coupled to NADH oxidation via myokinase, pyruvate kinase, and lactate dehydrogenase. Pantoate was prepared by incubating D-pantoyl lactone with an equimolar amount of NaOH for 20 min at 100 °C. The standard incubation mixture contained 100 mM buffer (as we describe below), 10 mM $MgCl_2$, 5 mM ATP, 5 mM pantoate, 10 mM β-alanine, 1 mM phosphoenolpyruvate, 0.36 μM NADH, myokinase (4 units), pyruvate kinase (6 units), lactate dehydrogenase (6 units), and PS (4 μg) in a final volume of 1 mL. The reaction was initiated by the addition of pantoate. An absorption change at 340 nm was monitored using a SHIMADZU UV-2500 spectrophotometer equipped with a temperature control unit. To investigate pH dependency of PS activity, the assay was carried out at 30 °C using the following buffer: Na-MES (pH 6.0−7.0), Na-HEPES (pH 7.0−8.0), Na-Bicine (pH 8.0−9.0), Na-CHES (pH 9.0−10.0), and Na-CAPS (pH 10.0−10.5), the concentrations of which were 100 mM. The temperature dependency of PS activity was explored in 100 mM Na-Bicine, pH 8.5. PS activity was determined by utilizing the absorption coefficient of NADH at 340 nm (6220 M^{-1} cm^{-1}). Experiments for each condition were repeated three times and averaged.

Crystallization and Data Collection. The purified sample was buffer-exchanged by dialysis against 50 mM Na-HEPES, pH 7.5, and 5 mM DTT and then concentrated to 10 mg/mL. Initial crystallization conditions were obtained with hanging-drop vapor diffusion using several crystal screening kits at 20 °C. Crystals appeared within 3 days under the conditions of 200 mM sodium formate, pH 7.0, 20% PEG3350 (no. 28), 200 mM sodium acetate, pH 7.0, 20% PEG3350 (no. 26), and 200 mM sodium bromide, 20% PEG3350 (no. 46) of the PEG/ION 2 crystal screen kit (Hampton Research). Optimization of these conditions yielded single crystals using a mixture of 3 μL of the proteins (10 mg/mL) and 3 μL of precipitant solution containing 10−12% PEG3350, 16−20% PEG400, and 200 mM sodium acetate, pH 9.0 at 20 °C. These crystals typically have the dimensions of 0.05 × 0.05 × 0.2 mm.

For cocrystallization with ATP and pantoate, a dialyzed sample was concentrated and incubated for 10 min at 4 °C in the presence of 10 mM ATP, 10 mM pantoate, and 5 mM $MgCl_2$. The final protein solution contained 50 mM Na-HEPES, pH 7.5, 5 mM DTT, 10 mM ATP, 10 mM pantoate, 5 mM $MgCl_2$, and 10 mg/mL protein. Crystallization was performed with hanging-drop vapor diffusion, and crystals appeared within 3 days under the conditions of the PEG/ION crystal screen kit 2. Optimization of these conditions yielded single crystals using a mixture of 3 μL of the proteins (8 mg/mL) and 3 μL of precipitant solution containing 10−12% PEG3350, 16−20% PEG400, 200 mM sodium acetate, pH 9.0, and 10 mM sodium iodide at 20 °C. These crystals typically have the dimensions of 0.05 × 0.05 × 0.2 mm.

The crystals used for refinement of the apoenzyme and cocrystal structures were mounted in a loop and then immediately flash-frozen in a cryostream of N_2 gas at 100 K. Diffraction data were collected at 100 K using the synchrotron radiation at SPring-8 (Japan). Data reduction and scaling were done with the program HKL2000 (*25*). Data processing statistics are listed in Table 1. The crystals of the apoenzyme and the cocrystals with ATP and pantoate belong to space groups $P6_5$ and $P2_1$, respectively.

Table 1: Data Collection and Refinement Statistics

	apoenzyme	PA complex
data collection		
radiation source	SPring-8 BL44XU	SPring-8 BL41XU
space group	$P6_5$	$P2_1$
cell dimensions (Å, deg)	131.7, 131.7, 89.2	46.0, 91.5, 87.3, 103.1
resolution range (Å)	114.0−2.5	85.1−1.85
no. of observed reflections	158004	218193
no. of unique reflections	30571	59235
completeness (%)	99.4 (97.8)[a]	98.3 (89.4)
I/σ(I)	17.5 (2.2)	5.7 (2.5)
R_{merge} (%)	4.3 (37.2)	9.1 (34.4)
refinement		
no. of amino acid residues (subunit A/B)	278/279	283/283
no. of water molecules	33	457
no. of other molecules[b]	0	12
no. of protein non-hydrogen atoms	4371	4442
R_{cryst} (%)	22.2	20.1
R_{free} (%)	24.1	22.8
average *B*-factor (Å^2)		
protein molecules	71.4	24.9
water molecules	49.0	33.2
rmsd		
bond lengths (Å)	0.0076	0.0055
bond angles (deg)	1.295	1.254
Ramachandran plot		
most favored/additionally allowed (%)	86.1/12.7	90.9/8.7
generously allowed (%)	0.8	0.4
disallowed (%)	0.4	0.0

[a]Highest resolution shell is shown in parentheses. [b]Pantoyl adenylate, acetate, and PEG400.

Molecular Replacement, Model Building, and Refinement. The crystal structure of the apoenzyme was determined by the molecular replacement (MR) method using the CCP4 program MOLREP (*26*) with the structure of subunit A of the *E. coli* PS (*17*) (PDB entry 1IHO) as a search model. The model refinement was carried out using the program CNS (*27*), with manual inspection and modification using the CCP4 program COOT (*28*, *29*). NCS averaging between two monomers within the dimer was attempted but did not improve the calculated electron density maps; thus, no NCS restraints were applied. After one round of simulated annealing, the CNS was used for positional and individual *B*-factor refinement (*27*).

To determine the structure of the enzyme cocrystallized with ATP and pantoate, the refined structure of the apoenzyme was used as a search model for the MR method. Initial attempts to solve the structure by the MR method with the structures of monomeric or dimeric apoenzymes were unsuccessful. A solution was obtained using the CCP4 program MOLREP by the following protocol: the structure of the N-terminal domain (residues 1−175) was first identified, and the molecules were fixed; a solution of the rotation and translation functions of the structure of the C-terminal domain (residue 176−283) was then obtained. After one round of simulated annealing, the CNS was used for positional and individual *B*-factor refinement (*27*). After solvent molecules had been incorporated into the structure, a Fourier difference synthesis revealed electron density clearly corresponding to the PA, which is the reaction intermediate formed by ATP and pantoate in the presence of Mg^{2+}. The complex with PA was subjected to additional rounds of structure

refinement with no NCS restraints. The stereochemistry of both structures was validated using the CCP4 program PROCHECK (*30*). The asymmetric units (ASUs) in the apoenzyme and the PA complex crystals contained one dimer each. The final atomic coordinates and structure factor amplitudes (PDB entries 3AG5 for the apoenzyme and 3AG6 for the PA complex) have been deposited in the Worldwide Protein Data Bank (wwPDB; http://www.wwpdb.org) and the Protein Data Bank Japan at the Institute for Protein Research in Osaka University (PDBj; http://www.pdbj.org/). The refinement statistics for both refined coordinate sets are presented in Table 1.

Analysis of Domain Movement. The movement of the domains of two PS structures was analyzed with the web-based program DynDom (*31*). In this analysis, the DynDom default settings were used as follows: the minimum domain size assigned was 20 residues, minimum ratio 1.0, and the sliding window length used was 5 residues. Hinge residues were identified at the transition point between the two dynamic domains.

RESULTS

Expression and Purification. The *S. aureus* NCTC8325 *panC* gene encoding the PS was cloned into a pCold TF expression vector, which produced PS protein fused to the protease-cleavable His_6 and trigger factor tag at its N-terminus. The recombinant protein was isolated from bacterial lysate by Ni^{2+}-affinity chromatography and cleaved with HRV 3C protease to remove the N-terminal tag. The digest results in the N-terminal addition of 18 amino acids. The digested enzyme was further purified to homogeneity with a yield of 1.3 mg of pure PS per 1 g of wet cells by using consecutive hydrophobic interaction chromatography and size exclusion chromatography. This system yielded a pure protein, judged by SDS−PAGE. The size exclusion chromatography profile demonstrated that the PS exists as a dimer in solution (data not shown), which is consistent with the previous observations of the enzymes from *E. coli* (*17*) and *M. tuberculosis* (*18*).

Optimum pH and Temperature. The recombinant enzyme activity was assayed to confirm the effect of an additional N-terminal peptide. Although purification and preliminary crystallographic analysis have been done for PS from *S. aureus* strain Sar2676 (*32*), the enzyme activity of *S. aureus* PS has not been reported to date. Our assay demonstrated that the k_{cat} value for *S. aureus* PS under the optimal condition (100 mM Na-Bicine, pH 8.5, 30 °C) was 1.5 s^{-1} (Figure 1), which is similar to those of the *E. coli* and *M. tuberculosis* PS enzymes (*14*, *16*, *33*). Further characterization demonstrated that the recombinant enzyme has a pH optimum between pH 8.0 and pH 9.0 and a temperature optimum of 30 °C (Figure 1). These enzymatic characteristics again are similar to the PS enzymes from other sources (*16*). The biochemical data confirmed that the additional N-terminal peptide in recombinant *S. aureus* PS has little effect on enzymatic activity.

Structure Solution. The model of the apoenzyme has been refined against data at 2.5 Å resolution to a crystallographic *R* factor of 22.2% (R_{free} of 24.1%) (Table 1). The ASU of the apoenzyme crystal contains two PS protomers (subunits A and B), which are roughly related by a noncrystallographic 2-fold axis with rmsds of 0.70 Å for the Cα atoms of the structured regions (Supporting Information Figure S2). The secondary structures of the two monomers in the ASU are highly similar. No electron density was observed for residues 65−69 of subunit A and 64−67 of subunit B of the apoenzyme, due to disordered structures in the

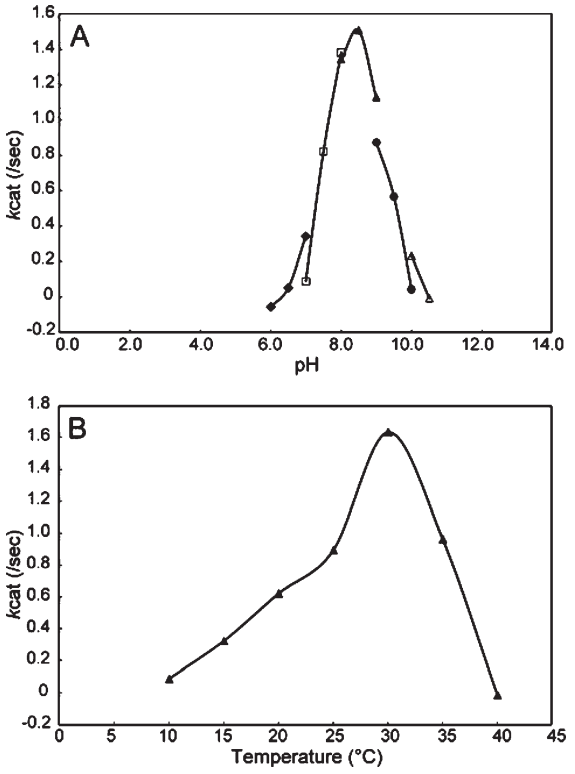

FIGURE 1: PS activity under various conditions. (A) pH and (B) temperature dependence of k_{cat} for *S. aureus* PS. (A) Assays were performed using various buffers at 30 °C. The k_{cat} values were plotted as squares (◆) for Na-MES, squares (□) for Na-HEPES, triangles (▲) for Na-Bicine, circles (●) for Na-CHES, and triangles (Δ) for Na-CAPS. (B) Assays were performed for 0.1 M Na-Bicine at pH 8.5. The optimal activity was observed at pH 8.5 in Na-Bicine.

crystals. The extra 18 residues at the N-terminus are also structurally disordered. The final model of the apoenzyme contains 557 of 566 expected residues of the dimer and 33 water molecules. The Wilson *B*-factor of the data (60.9 $Å^2$) is comparable to the average *B*-factor of the model (71.4 $Å^2$).

The cocrystal structure has been refined against data at 1.85 Å resolution to a crystallographic *R* factor of 20.1% (R_{free} of 22.8%) (Table 1). This crystal also contains two PS monomers per ASU (subunits A and B), which are roughly related by a noncrystallographic 2-fold axis with rmsds of 0.46 Å for the Cα atoms (Supporting Information Figure S2). The two monomers in the ASU have highly similar secondary structures, and some structural elements differ from those of the apoenzyme (Figure 2). All of the residues of subunits A and B (residues 1−283) of the cocrystal structure could be readily traced. The electron density showed a PA molecule in each active site. The two PA molecules have average temperature factors of 23.0 and 25.9 $Å^2$, which are virtually identical to the average temperature factors of the surrounding protein atoms. This result suggests that the active sites of the cocrystal structure are fully occupied by PA. It is worth noting that the active site also accommodates an acetate molecule, which is contained in the crystallization solution as a precipitant. Acetate could not be found except for the active site, although there is 200 mM acetate in the crystallization solution. The eight PEG400 molecules used as a precipitant in crystallization are bound to the molecular surface (Supporting Information Figure S1). The final model of the PA complex contains 566 amino acid residues, as well as two PA, two acetate, eight PEG400, and 457 water molecules. The Wilson *B*-factor of the

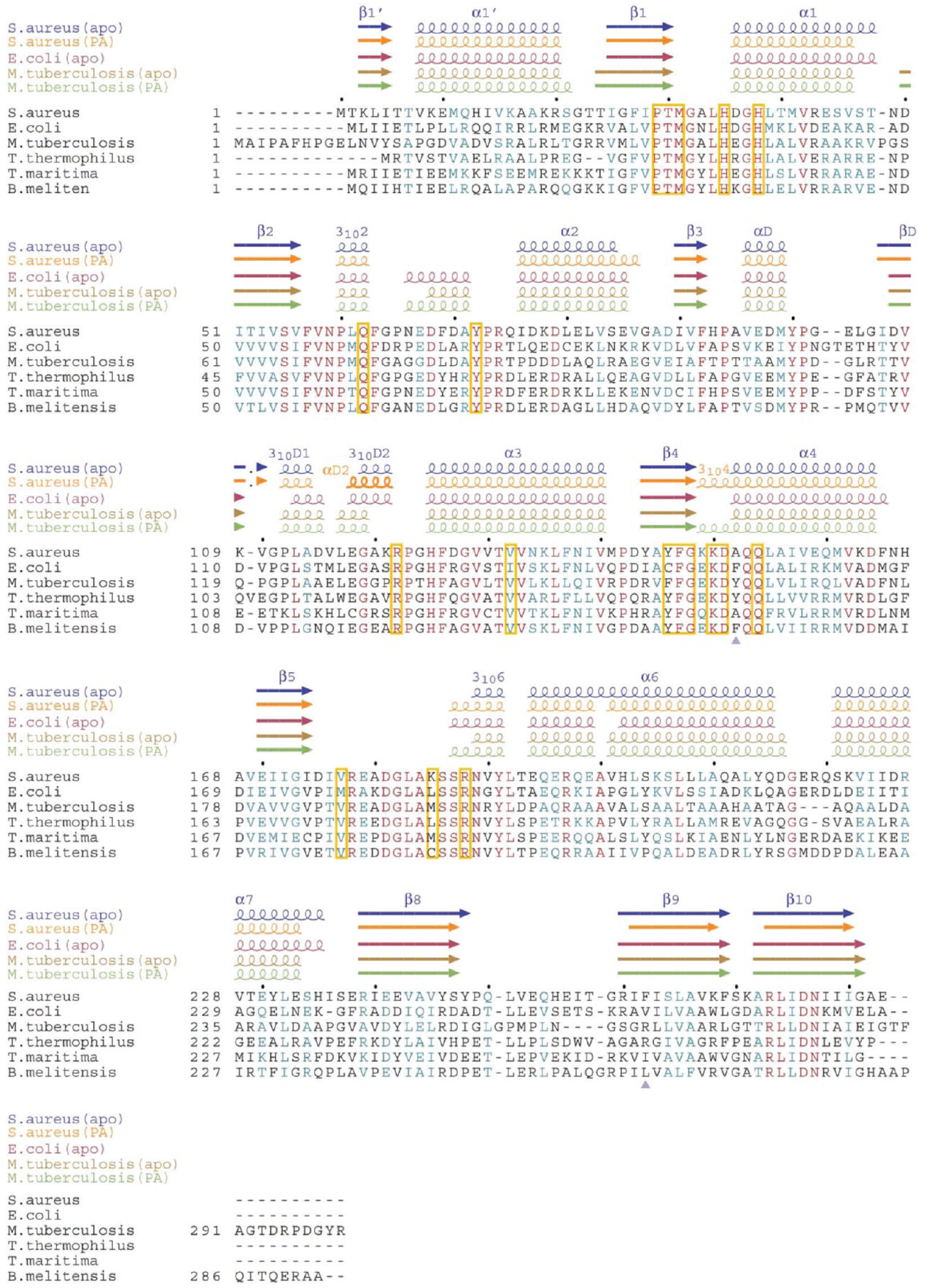

FIGURE 2: Sequence alignment among PS proteins. Sequences were aligned with CLUSTALW (*35*), and this figure was generated using ESPript (*36*). Identical residues are highlighted in red, whereas the light blue color denotes similar sequences. The residues discussed in this paper are surrounded by the yellow squares. Helices of the structures are denoted by coils, and β-strands of those are denoted by arrows. The secondary structural elements of *S. aureus* PS enzymes, the apoenzyme of *E. coli* PS (PDB entry 1IHO), the apoenzyme (PDB entry 3COV), and the PA complex (PDB entry 1N2H) of *M. tuberculosis* PS were determined with the program DSSP (*37*). The triangles (▲) indicate the residues involved in the steric hindrance between the N- and C-terminal domains.

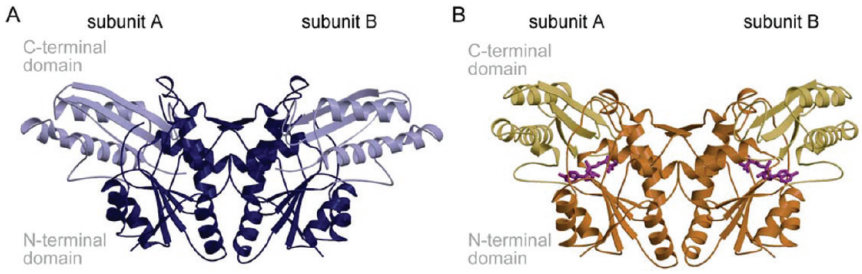

FIGURE 3: Ribbon diagrams of the apoenzyme and the PA complex of *S. aureus* PS dimer. (A) The N-terminal domains of the apoenzyme are in blue, and the C-terminal domains are in light blue. (B) The N-terminal domains of the PA complex are in orange, and the C-terminal domain is in yellow.

data (21.1 Å^2) is comparable to the average *B*-factor of the model (24.9 Å^2).

In the apo structure, one residue (Leu117) has angles (subunit A, $\psi = 75°$, $\varphi = 54°$; subunit B, $\psi = 65°$, $\varphi = 52°$) in the disallowed region of the Ramachandran plot (*34*), whereas all main chain dihedrals fall within the most favorable, additionally allowed, and generously allowed regions in the PA complex (Table 1). Leu117 lies in areas of well-defined electron density in both the apoenzyme and the PA complex. Leu117 is located next to the short 3_{10} helix (residues 112−114) in subunit A of the apoenzyme, while the residue is sandwiched between two short 3_{10} helices (residues 112−114 and 119−121) in subunit B. The latter 3_{10} helix (residues 119−121) becomes a regular α-helix when PA is bound (discussed in detail later). The structures of *E. coli* and *M. tuberculosis* PS enzymes indicate that the equivalent residues (Leu118 in *E. coli* PS and Leu127 in *M. tuberculosis* PS) in the apo structure are located in a similar region of the Ramachandran plot and are also located next to the equivalent 3_{10} helix (Figure 2), suggesting that structural features are shared among *E. coli* (*17*), *M. tuberculosis* (*18*, *19*), *and S. aureus* PS enzymes.

Overall Structure. The crystal structure of the *S. aureus* PS enzyme exhibits a dimer (Figure 3A), which is in good agreement with the molecular weight estimated by size exclusion chromatography. The dimeric structure of the *S. aureus* PS resembles a butterfly (Figure 3A), and the dimeric quaternary architecture is basically the same as that of *M. tuberculosis* and *E. coli* PS enzymes (*17*−*19*). The PS monomer consists of two well-defined domains, the N-terminal domain (residues 1−175) and the C-terminal domain (residues 176−283) connected by a hinge region. The subunit has an α/β architecture, in which the N-terminal domain adopts a Rossmann fold, and the C-terminal domain consists of a three-stranded antiparallel β-sheet and two α-helices (Figure 4A). The apo structure represents an open state of the enzyme (Figure 3A), as the active site is solvent-accessible (Figure 4C) and the catalytically essential residues are spatially separated into domains (Figure 4A). On the other hand, the PA complex structure adopts a closed conformation (Figure 3B), expected to be catalytically relevant. The active site of the PA complex is almost embedded within the molecule (Figure 4D).

The C-terminal domains of the apoenzyme appear to be flexible, with poorly resolved electron density and high crystallographic temperature factors (average Cα temperature factors of 72.6 Å^2 for subunit A and 100.2 Å^2 for subunit B), compared to those of the N-terminal domains (58.0 Å^2 for subunit A and 62.4 Å^2 for subunits B). In the overall structure, the three regions are particularly highly mobile. The first region is the loop (residues 57−75) between β2 and α2 (Figures 2 and 4A). This region corresponds to a loop (residue 74−88) in *M. tuberculosis* PS, which has been proposed to function as a gate to the active site cavity (*18*, *19*). In the same way, this disordered loop of *S. aureus* PS also became ordered in the PA complex structure, suggesting that this loop may be functionally similar to that of *M. tuberculosis* PS. The second is the region (residues 111−124) containing the two short 3_{10} helices between βD and α3 (Figures 2 and 4A) with average Cα temperature factors of 92.9 Å^2 for subunit A and 89.6 Å^2 for subunit B, respectively. In the PA complex, this region is consolidated by several interactions with the C-terminal domain (e.g., Glu118 to Arg273) to undergo a conformational disorder-to-order transition. The latter half of this region (residues 118−121) becomes a regular α-helix (αD2) with low temperature factors upon ligand binding (Figures 2 and 4B). The third is the two helices (α6 to α7) in the C-terminal domain of subunit B (average Cα temperature factor of 114.4 Å^2), but the equivalent region of subunit A has a relatively low temperature factor (average Cα temperature factor of 72.0 Å^2). This is likely caused by the differences in crystal packing contacts, because subunit A contacts a neighboring molecule in the crystal whereas subunit B does not.

Unlike the apo structure, the structure of the PA complex is entirely well-defined with relatively low temperature factors (average Cα temperature factor is 23.7 Å^2). The N- and C-terminal domains of the PA complex have similar average Cα temperature factors of 22.2 and 26.1 Å^2, respectively. The highly mobile regions in the apo structure are virtually ordered in the PA complex structure. The region (residues 57−75) forms structurally ordered β2 and α2. The side chain Gln62 in this region participates in direct interaction with PA (Figure 5A,B), thereby stabilizing the active site of the PA complex. The above-described region (residues 111−124) and the two helices (α6 to α7) of the C-terminal domain also have relatively low temperature factors of 20.6 and 25.8 Å^2 for residues 111−124 and α6 to α7, and both of the values are comparable to the overall average temperature factors. Thus, the presence of bound PA leads to a rigid structure; however, in the absence of the reaction intermediate, the structure adopts a more open and flexible conformation.

Dimerization. The ASU of the apoenzyme crystal and that of PA complex crystal each contain one functional dimer with two well-defined domains per monomer. In the apo structure, the N- and C-terminal domains can be superimposed on each other (rmsd of 0.8 Å over 170 aligned Cα atoms for the N-terminal domain, and 0.51 Å over 108 aligned Cα atoms for the C-terminal domain), while those of PA complex can be superimposed on each other (rmsd of 175 Cα positions and 0.32 Å for the N-terminal domain, and 108 Cα positions 0.30 Å for the C-terminal domain). However, the structures of the two protomers in the ASUs are not completely identical for both of the crystals. In both of the structures, the C-terminal domains differ slightly in orientation relative to the N-terminal

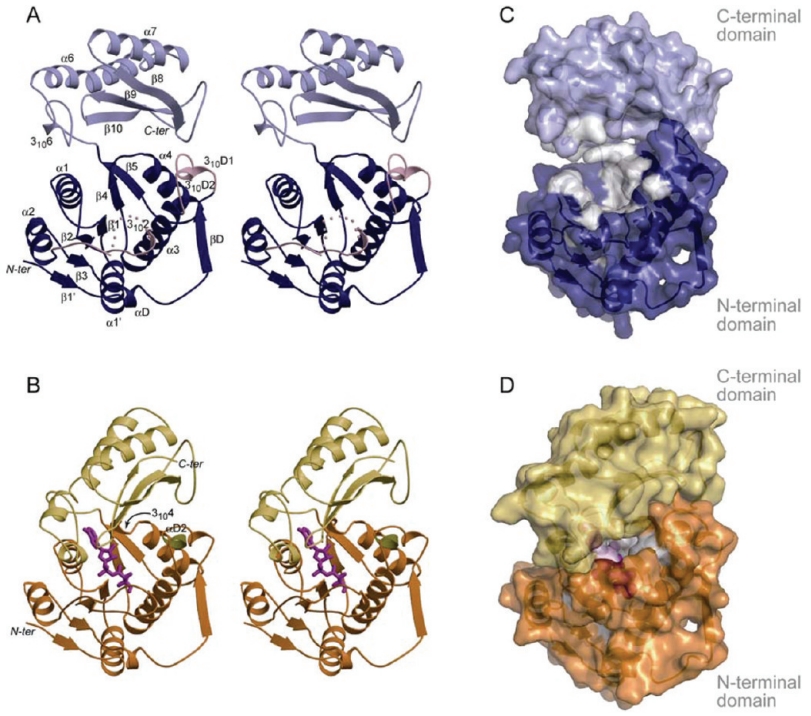

FIGURE 4: Monomer structure of *S. aureus* PS in the apoenzyme and the PA complex. (A, B) Stereo cartoon of the apoenzyme and the PA complex monomer. Relative to Figure 3B, the molecule was rotated 45° clockwise around the vertical axis. Color coding and display of the ribbons are the same as in Figure 3. The loops (residues 57−75 and 111−124) are colored in pink, and an internal disordered region is shown as a dotted line. (C, D) Apoenzyme and PA complex monomer. The residues involved in PA binding are in white. The region (residues 119−121) is colored in olive green.

domains. Observation indicates that the symmetry axes that relate the N- and C-terminal domains are not equivalent in the apoenzyme and the PA complex structures. This feature resembles those of *M. tuberculosis* and *E. coli* PS enzymes (*17*−*19*).

The dimer interface of both the apoenzyme and the PA complex is extensive, with the apoenzyme having a buried area of 2850 Å^2 and with that of the PA complex having a buried area of 2800 Å^2, calculated with the CCP4 program AREAIMOL (*28*). Intersubunit interactions are also roughly conserved in the apo and the PA complex structures, involving more than 30 residues of the N-terminal domains. Of those, a remarkable feature is the intersubunit two-stranded antiparallel β-sheet (residues 106−110). In addition, extensive interactions are found in the region (residues 164−166), which makes contact with Gln12, Gly105, Ile106, Lys135, and Asn138 of the other subunit. Additionally, Asn134 and Asn138 extensively interact with Asn134, Asn138, Phe165, and His167 of the other subunit via bridging water molecules.

Active Site Structure. Crystal structures of *M. tuberculosis* PS revealed that the active sites of both the apoenzyme and the PA complex are almost embedded into the molecule. In contrast, the active site of the apoenzyme of *S. aureus* PS is exposed to the solvent (Figure 4C), in the same manner as that of *E. coli* (*17*). The side chain of Arg188, which is believed to be responsible for both ATP and β-alanine binding, is located approximately 10 Å from the predicted substrate binding site in the N-terminal domain (Supporting Information Figure S4). Therefore, the structure of the apoenzyme of *S. aureus* appears poised in the unobstructed conformation, ready to accept available substrates.

In the PA complex, the active site is shielded from the solvent (Figure 4D), so that PA and acetate are sequestered in the active site pocket. The residues involved in binding PA can be divided into two groups: those interacting with the pantoyl group of PA and those interacting with the adenylate group of PA. The residues belonging to the former group are listed as follows: the side chains of Gln62 and Gln154 that are hydrogen bonded to the pantoyl group, the backbones of Pro29 and Thr30, and the side chains of Val132 and Phe147 that form hydrophobic interactions with methylene carbon of the pantoyl group (Figure 5A,B). Additionally, there are several water-mediated hydrogen bonds to the pantoyl group. The residues participating in binding of the adenylate group are more extensive: Met31, His35, His38, Tyr72, Tyr146, Gly148, Asp151, Val177, and Lys185 are involved in the binding of the adenylate group. Of these, the backbone amide and carbonyl of Val177 appear to play a key role in the domain movement, as discussed later. Except for the above-mentioned residues, the adenine aromatic face makes a stacking contact with the aliphatic portion of the Lys150. Lys150 has been proposed to interact with β-phosphate of ATP in the first condensation reaction (*18*, *33*). In the apo structure, the side chain of Lys150 on the loop (residues 149−151) is exposed to solvent. With PA bound, new hydrogen bonds are formed between the backbone carbonyls of Lys149 and Lys150 (from the N-terminal domain) and the side chain of Asn277 (from the C-terminal domain) to drive the domain closure. This then forms a 3_{10} helix of the region (residues 149−151), which adopts the loop structure separated by β4 and α4 in the apoenzyme. The domain closure rearranges the interactions involved in the neighboring residues. In the apoenzyme, the side chain of Asp151 is hydrogen bonded to the backbone amides of Ala152, Glu153, and Gln154. In the PA complex, the side chain of Asp151 directly participates in binding PA and in forming the tunnel of predicted substrate pathway, implying that the Asp151 might determine the orientation of substrate β-alanine so as to achieve a nucleophilic attack.

Strikingly, an acetate molecule is bound in the vicinity of PA. The carboxyl group of the acetate forms hydrogen bonds to the

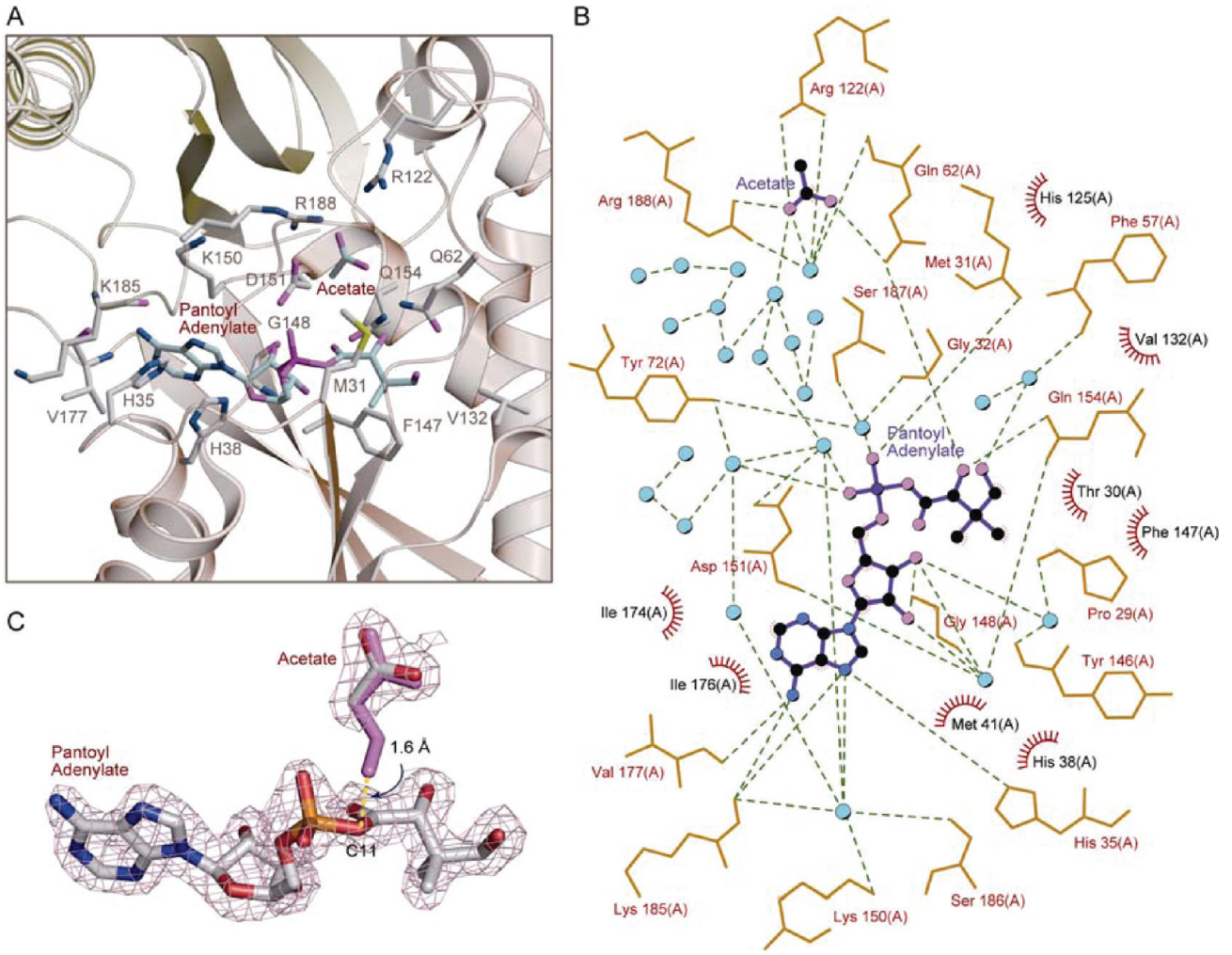

FIGURE 5: Active site in the PA complex. (A) The view of the active site is shown with PA, acetate, and residues that are involved in PA and acetate binding. Color coding of the protein side chains is by atom type with the carbons in white, oxygens in pink, nitrogens in blue, and phosphorus in red, and the carbons of PA and acetate are colored in cyan. (B) LIGPLOT (*38*) diagram of the active site of the PA complex. Color coding of the PA molecule is by atom type with the carbons in black, oxygens in pink, nitrogens in blue, and phosphorus in purple. Water molecules are shown in cyan balls. Hydrogen bonds are indicated by green dotted lines, and hydrophobic interactions are represented as barbed circle sections. (C) $F_o - F_c$ omit map and β-alanine model. The carbons of the modeled β-alanine are colored in pink. The $F_o - F_c$ map are contoured at 2.0σ, generated before inclusion of PA and acetate in the model.

side chains of Gln62, Arg122, and Arg188 (Figure 5A,B). The methyl group of the acetate molecule is located 4.2 Å apart from the C11 of PA. The residues involved in binding PA and acetate are highly conserved in all PS enzymes, except Val132, Tyr146, Val177, and Lys185 (Figure 2). The nonconserved residues except for Val132 (Ile in *E. coli* enzyme) interact via only backbone amide or carbonyl, suggesting that all PS enzymes shares a common reaction mechanism.

Domain Movement upon Substrate Binding. Although the subunit structures of the apoenzyme and the PA complex cannot be closely superimposed (rmsd of 3.9 Å over 278 aligned Cα atoms), individual domains can be superimposed well (rmsd of 0.7 Å over 170 aligned Cα atoms for the N-terminal domain, and 0.9 Å over 108 aligned Cα atoms for the C-terminal domain), indicating that a large domain movement occurs when PA is bound. From this structural analysis, therefore, the first direct evidence has been obtained of a hinge bending domain closure in PS (Figure 6A), as was proposed for the *E. coli* PS (*17*).

When the movement of the domains was analyzed by the program DynDom (*31*), the following results were obtained. The conformational changes can be described as the rigid body movement of two domains (rotation of 37°) (Figure 6B). The two identified rigid domains are composed of residues 1−175 and residues 176−283, which roughly correspond to the N- and C-terminal domains. The region (residues 174−176) was identified as the "bending residues" between the two domains.

The domain movement leads to the rearrangement of the hydrogen bond network between the N- and C-terminal domains. In the apoenzyme, the interdomain interactions are mainly made by hydrophobic residues such as Leu117, Ala152, Gln153, Asp175 (N-terminal domain), Ile176, Tyr246, Leu251, and Phe262 (C-terminal domain), although two hydrogen-bonding interactions are found between the side chain of Asn277 and the backbone carbonyl of Lys150 and between the side chain of Glu159 and the side chain of Tyr248. As described in "Active Site Structure", Lys150 may play a crucial role in the first condensation reaction (*18*, *33*). When PA is bound, the side chain of Tyr248, which interacts with Glu159 in the apoenzyme, swings to interact with the backbone carbonyl of Ala152. Additional interactions are found between the side chain of Tyr191 and Asp68 (2.8 Å), the side chain of Asp68 and Arg188 (2.8 Å), the side chain of Asn277 and the backbone carbonyl of

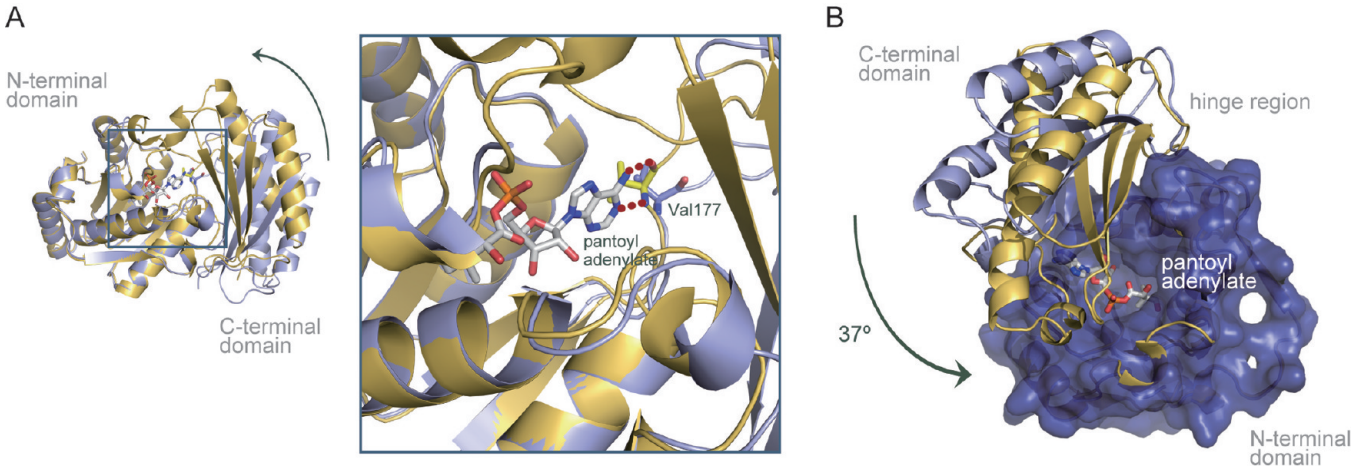

FIGURE 6: Superposition of the apoenzyme and the PA complex of *S. aureus* PS. (A) Illustration of the potential role of Val177 in triggering domain movement. The interaction between the adenine ring of PA and Val177 is shown (red dotted line). (B) The structures of the apoenzyme and the PA complex were superimposed based on the N-terminal domains. PA is shown as stick models. The N-terminal domain of the apoenzyme is represented by the blue surface, and C-terminal domains are shown as ribbon diagrams, showing the 37° rotation of the C-terminal domain.

Lys149 (3.1 Å), and the side chain of Ser 187 and the backbone carbonyls of Gly32 and Ala33 (3.2 and 2.5 Å). A salt bridge between the side chains of Glu118 and Arg273 was also formed. In addition, many water-mediated interactions are generated by the domain movement.

Together with the newly generated interactions, the domain movement induces disorder-to-order transitions. Asp68 is located in the disordered region in the apoenzyme, while the side chain of Asp68 of the PA complex directly interacts with Arg188 and Tyr191 to undergo the disorder-to-order transition of region 65−69. Because previous structural studies revealed that Arg188 directly participates in binding of ATP (the first substrate) and β-alanine (the third substrate) (*18*, *19*), the disorder-to-order transition of Asp68 must be crucial for the multiple states in the enzymatic reactions. In the PA complex, the side chain of Glu67 is salt-bridged to the side chain of Arg122, which directly participates in acetate binding.

The region (residues 118−122) with the high temperature factors in the apoenzyme conserves polar residues such as Glu118, Lys121, and Arg122. This region also becomes ordered when PA is bound. Consequently, these polar residues appear to constitute the entrance of the active site cavity in the PA complex (Supporting Information Figure S5). Glu118 is salt-bridged to the side chain of Arg273, thereby connecting the N- and C-terminal domains.

DISCUSSION

Mechanism of PA-Induced Domain Movement. When the overall structures of the apoenzyme and the PA complex of *S. aureus* PS are superimposed based on the N-terminal domains, a slight but significant structural difference is observed at the linker (residues 174−176) between the N- and C-terminal domains (Figure 6A). This superimposition reveals that the interactions between the adenine ring of PA and the backbone amide and carbonyl of Val177 are newly formed when PA is bound, which is likely to trigger a large structural transition. This is also consistent with DynDom analysis, which indicated that the region (residues 174−176) is identified as containing the "bending residues". Since ATP is the first substrate in the reaction (Scheme 1), it is thus tempting to speculate that the first substrate ATP would trigger the domain movement, although this hypothesis must be proven by solving the *S. aureus* PS structure in complex with ATP or ATP analogues.

Acetate as a Substrate Analogue. The modeled structure of β-alanine (the third substrate) based on acetate indicates the amino group of β-alanine is positioned 1.6 Å apart from the C11 of PA (Figure 5C), which is close enough to achieve a nucleophilic attack. Therefore, we infer that the acetate mimics the substrate β-alanine, indicating that the PA complex structure corresponds to a catalytic state poised for the nucleophilic attack of β-alanine on PA in the enzymatic reaction (Scheme 1). Although the crystal structures of the various complexes of *M. tuberculosis* PS have been reported (*18*, *19*, *21*, *22*), no reports on the structures of PA together with the β-alanine analogues are available so far. The crystal structure of the β-alanine−AMP complex of *M. tuberculosis* PS (PDB entry 2A86) has been reported, but this state does not coincide with the catalytic mechanism to be bi-uni uni-bi ping-pong. The acetate binds to the similar position of the carboxylate of β-alanine in the β-alanine−AMP complex of *M. tuberculosis* PS (Supporting Information Figure S3). Assuming that acetate mimics β-alanine, the complex structure represents a catalytic state in the PS reaction. This structure exhibits the detailed binding structure of β-alanine in the presence of PA, which is different from that of the β-alanine−AMP complex (*18*). For example, in the *S. aureus* PS complex, the side chains of Gln62, Arg122, and Arg188 tightly bind to the carboxyl group of the acetate with distances of 2.7, 2.9, and 3.0 Å, respectively, whereas the side chains of corresponding residues are positioned with distances of 2.9, 8.5, and 4.1 Å in the *M. tuberculosis* PS β-alanine−AMP complex.

Distinct Modes of Domain Movement for S. aureus and M. tuberculosis PS Enzymes. Whereas the overall structure of the PA complex of *S. aureus* PS closely resembles that of the PA complex of *M. tuberculosis* PS (rmsd of 2.3 Å over 278 aligned Cα atoms), the structure of the apoenzyme of *S. aureus* PS cannot be superimposed well on that of *M. tuberculosis* PS. The comparison suggests that *S. aureus* PS undergoes open/close conformational change upon substrate binding, while *M. tuberculosis* PS is retained with no large transition (close/close). As the apoenzyme of *E. coli* adopts an open structure (*17*), the open/close mechanisms might be shared in both *S. aureus* and *E. coli* PS enzymes. A question naturally arises as to why *S. aureus* PS (probably *E. coli* PS as well) has the open/close transition, whereas *M. tuberculosis*

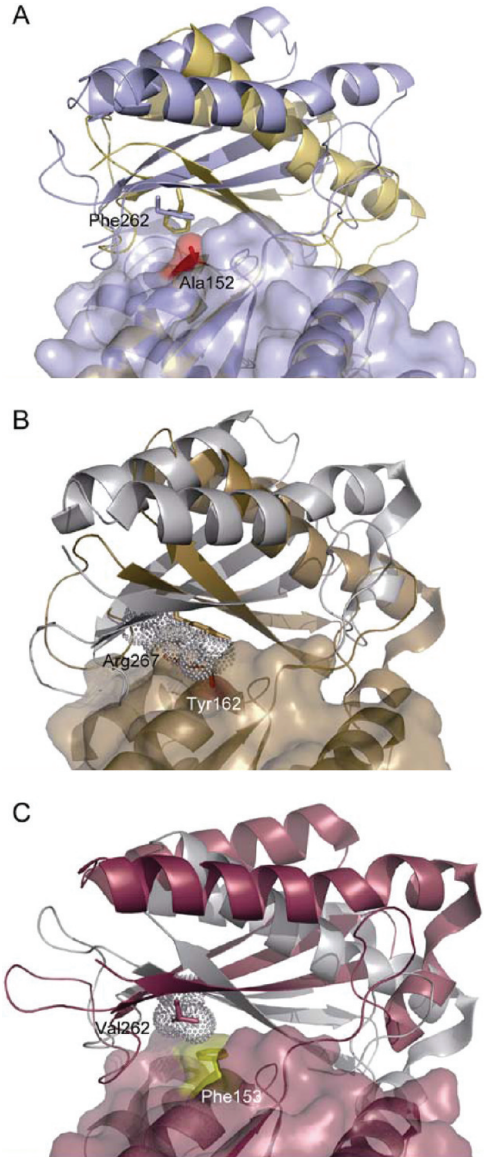

FIGURE 7: Modeled structures of PS enzymes. PS enzymes of *S. aureus* (A), *M. tuberculosis* (B) (PDB entry 3COV), and *E. coli* (C) (PDB entry 1IHO) are shown. The apo and PA complex structures of *S. aureus* PS are colored in yellow and light blue, respectively. The modeled structures in (B) and (C) are colored in white. The residues of N- and C-terminal domains involved in the steric hindrance are shown as red surface and space-filled sphere models, respectively, and the residues are labeled.

PS does not. It is unlikely that the domain movement arises from inherent structural propensities of the linker between the N- and C-terminal domains, because no obvious correlation between their sequences of the linker (residues 174−176) and the hinge bending domain closure is observed among the three PS enzymes (Figure 2).

Wang et al. proposed that relatively tight interdomain interactions, including two salt bridges (Arg253 to Glu126 and Arg267 to Glu159), might contribute to fix the relative positions of the N- and C-terminal domains in *M. tuberculosis* PS (*18*). Such tight interactions are not found at the interface of the domains of the apo structures of *S. aureus* and *E. coli* PS enzymes. However, this hypothesis is not fully consistent with the other PS homologues of *T. thermophilus* HB8 and *T. maritima*. The structures of these homologues have been deposited as apoenzymes, both of which adopt the closed structures. *T. thermophilus* HB8 PS homologue only conserves the latter salt bridge (Arg256 to Glu144), and *T. maritima* PS homologue has neither of them. In addition to the interactions, we propose that the steric hindrance between the N- and C-terminal domains may be a determinant of the domain movement characteristics. In Figure 2, the residues involved in the steric hindrance are shown as triangles. In *S. aureus* PS, the close to open transition generates new interdomain interactions. Of those, Phe262 approaches Ala152 to make a hydrophobic interaction between the side chains upon the close to open transition (Figure 7A). However, if the open form of *M. tuberculosis* PS is modeled by rigid-body fitting using the apo structure of *S. aureus* PS, the model produces steric hindrance, because the corresponding residues of *M. tuberculosis* PS are more bulky (Tyr162 and Arg267) (Figure 7B), and Arg267 is also involved in the interdomain salt bridge. Thus, the steric hindrance can explain why *M. tuberculosis* PS cannot adopt an open structure. If the closed form of the *E. coli* PS is modeled by rigid-body fitting using the PA complex structure of *S. aureus* PS, no steric hindrance is found between the N- and C-terminal domains (Figure 7C). Similarly, the structures of the PS homologue of *T. thermophilus* HB8 (PDB entries 1UFV and 1V8F) are consistent with the proposal (Supporting Information Figure S6). An exception is the apoenzyme of *T. maritima* PS that is expected to adopt an open structure, based on our proposal, but the crystal structure is closed. It can be explained by the several other interdomain interactions (see Supporting Information Figure S6). The coordinates of *B. melitensis* PS homologue (PDB entry 3INN), which have been deposited as ATP complex, show the closed structure. *B. melitensis* PS homologue has neither tight interdomain interactions proposed by Wang et al. nor steric hindrance (Supporting Information Figure S6); therefore, *B. melitensis* PS homologue might undergo open/close conformational change. Since models generated by rigid-body fitting without adequate atomic fitting can be unreliable, whether such features characterize the hinge bending closure of PS enzymes awaits further mutagenesis studies.

Toward Developing New Inhibitors. The structures of the apoenzyme and the PA complex of *S. aureus* PS provide not only a detailed view of the domain movement but also the detailed structure of how PA and acetate are bound, which represents a catalytic state in the enzymatic reaction. Studies of the intermediate-based drug design are currently underway for *M. tuberculosis* PS (*21*, *22*), and the PA-based approach seems to be very effective. For example, nonhydrolyzable PA-mimicking compounds effectively inhibit the activity of *M. tuberculosis* PS (*21*, *22*). We anticipate that a PA-based approach in combination with acetate would be ideal for new compounds that selectively inhibit PS activity. Additionally, a compound that binds tightly to the hinge region would hamper the hinge movement, which points the way to an innovative strategy for designing a novel inhibitor for *S. aureus* PS.

ACKNOWLEDGMENT

We thank Prof. Duncan Maskell, University of Cambridge, for the gift of *S. aureus* DNA and Drs. Sukanta Moldal and Kenji Mizuguchi, National Institute of Biomedical Innovation, for carefully reading the manuscript.

SUPPORTING INFORMATION AVAILABLE

Binding structure of PEG400, shift of each Cα when the two protomers in the ASU are superimposed, superimposition of the active sites of *S. aureus* PS and *M. tuberculosis* PS, ATP-binding

models, electrostatic surface of the PA complex, and modeled structures of PS homologues of *T. thermophilus* HB8, *T. maritima*, and *B. melitensis* are all available free of charge via the Internet at http://pubs.acs.org.

REFERENCES

1. Nieidhardt, F. (1996) Escherichia coli and Salmonella typhimurim: cellular and molecular biology, Vol. *1*, American Society for Microbiology, Washington, DC.
2. Abiko, Y. (1975) Metabolism of Coenzyme A, in Metabolic Pathway, Vol. *1*, Academic Press, New York.
3. Mishra, P. K., and Drueckhammer, D. G. (2000) Coenzyme A analogues and derivatives: synthesis and applications as mechanistic probes of coenzyme A ester-utilizing enzymes. *Chem. Rev. 100*, 3283–3310.
4. DiRusso, C. C., Heimert, T. L., and Metzger, A. K. (1992) Characterization of FadR, a global transcriptional regulator of fatty acid metabolism in *Escherichia coli*. Interaction with the fadB promoter is prevented by long chain fatty acyl coenzyme A. *J. Biol. Chem. 267*, 8685–8691.
5. Korchak, H. M., Kane, L. H., Rossi, M. W., and Corkey, B. E. (1994) Long chain acyl coenzyme A and signaling in neutrophils. An inhibitor of acyl coenzyme A synthetase, triacsin C, inhibits superoxide anion generation and degranulation by human neutrophils. *J. Biol. Chem. 269*, 30281–30287.
6. Dreier, J., Shah, A. N., and Khosla, C. (1999) Kinetic analysis of the actinorhodin aromatic polyketide synthase. *J. Biol. Chem. 274*, 25108–25112.
7. Lambalot, R. H., Gehring, A. M., Flugel, R. S., Zuber, P., LaCelle, M., Marahiel, M. A., Reid, R., Khosla, C., and Walsh, C. T. (1996) A new enzyme superfamily—the phosphopantetheinyl transferases. *Chem. Biol. 3*, 923–936.
8. Genschel, U. (2004) Coenzyme A biosynthesis: reconstruction of the pathway in archaea and an evolutionary scenario based on comparative genomics. *Mol. Biol. Evol. 21*, 1242–1251.
9. Sambandamurthy, V. K., Wang, X., Chen, B., Russell, R. G., Derrick, S., Collins, F. M., Morris, S. L., and Jacobs, W. R., Jr. (2002) A pantothenate auxotroph of *Mycobacterium tuberculosis* is highly attenuated and protects mice against tuberculosis. *Nat. Med. 8*, 1171–1174.
10. Seetharamappa, J., Oke, M., Liu, H., McMahon, S. A., Johnson, K. A., Carter, L., Dorward, M., Zawadzki, M., Overton, I. M., van Niekirk, C. A., Graham, S., Botting, C. H., Taylor, G. L., White, M. F., Barton, G. J., Coote, P. J., and Naismith, J. H. (2007) Purification, crystallization and data collection of methicillin-resistant *Staphylococcus aureus* Sar2676, a pantothenate synthetase. *Acta Crystallogr., Sect. F: Struct. Biol. Cryst. Commun. 63*, 488–491.
11. Merkel, W. K., and Nichols, B. P. (1996) Characterization and sequence of the *Escherichia coli* panBCD gene cluster. *FEMS Microbiol. Lett. 143*, 247–252.
12. Webb, M. E., Smith, A. G., and Abell, C. (2004) Biosynthesis of pantothenate. *Nat. Prod. Rep. 21*, 695–721.
13. Miyatake, K., Nakano, Y., and Kitaoka, S. (1978) Enzymological properties of pantothenate synthetase from *Escherichia coli* B. *J. Nutr. Sci. Vitaminol.* (*Tokyo*) *24*, 243–253.
14. Zheng, R., and Blanchard, J. S. (2001) Steady-state and pre-steady-state kinetic analysis of *Mycobacterium tuberculosis* pantothenate synthetase. *Biochemistry 40*, 12904–12912.
15. Genschel, U., Powell, C. A., Abell, C., and Smith, A. G. (1999) The final step of pantothenate biosynthesis in higher plants: cloning and characterization of pantothenate synthetase from *Lotus japonicus* and *Oryza sativum* (rice). *Biochem. J. 341* (Part 3), 669–678.
16. Jonczyk, R., and Genschel, U. (2006) Molecular adaptation and allostery in plant pantothenate synthetases. *J. Biol. Chem. 281*, 37435–37446.
17. von Delft, F., Lewendon, A., Dhanaraj, V., Blundell, T. L., Abell, C., and Smith, A. G. (2001) The crystal structure of *E. coli* pantothenate synthetase confirms it as a member of the cytidylyltransferase superfamily. *Structure 9*, 439–450.
18. Wang, S., and Eisenberg, D. (2003) Crystal structures of a pantothenate synthetase from *M. tuberculosis* and its complexes with substrates and a reaction intermediate. *Protein Sci. 12*, 1097–1108.
19. Wang, S., and Eisenberg, D. (2006) Crystal structure of the pantothenate synthetase from *Mycobacterium tuberculosis*, snapshots of the enzyme in action. *Biochemistry 45*, 1554–1561.
20. Chakrabarti, K. S., Thakur, K. G., Gopal, B., and Sarma, S. P. (2010) X-ray crystallographic and NMR studies of pantothenate synthetase provide insights into the mechanism of homotropic inhibition by pantoate. *FEBS J. 277*, 697–712.
21. Ciulli, A., Scott, D. E., Ando, M., Reyes, F., Saldanha, S. A., Tuck, K. L., Chirgadze, D. Y., Blundell, T. L., and Abell, C. (2008) Inhibition of *Mycobacterium tuberculosis* pantothenate synthetase by analogues of the reaction intermediate. *ChemBioChem 9*, 2606–2611.
22. Scott, D. E., Dawes, G. J., Ando, M., Abell, C., and Ciulli, A. (2009) A fragment-based approach to probing adenosine recognition sites by using dynamic combinatorial chemistry. *ChemBioChem 10*, 2772–2779.
23. Velaparthi, S., Brunsteiner, M., Uddin, R., Wan, B., Franzblau, S. G., and Petukhov, P. A. (2008) 5-*tert*-Butyl-*N*-pyrazol-4-yl-4,5,6,7-tetrahydrobenzo[*d*]isoxazole-3-carboxamide derivatives as novel potent inhibitors of *Mycobacterium tuberculosis* pantothenate synthetase: initiating a quest for new antitubercular drugs. *J. Med. Chem. 51*, 1999–2002.
24. White, E. L., Southworth, K., Ross, L., Cooley, S., Gill, R. B., Sosa, M. I., Manouvakhova, A., Rasmussen, L., Goulding, C., Eisenberg, D., and Fletcher, T. M., III (2007) A novel inhibitor of *Mycobacterium tuberculosis* pantothenate synthetase. *J. Biomol. Screen. 12*, 100–105.
25. Otwinowski, Z. (1993) Oscillation data reduction program, in Data Collection and Processing: Proceedings of the CCP4 Study Weekend: Data Collection and Processing (Sawyer, L., Isaacs, N., and Bailey, S., Eds.) pp 56−62, Daresbury Laboratory, Warrington, U.K.
26. Vagin, A., and Teplyakov, A. (1997) MOLREP: an automated program for molecular replacement. *J. Appl. Crystallogr. 30*, 1022–1025.
27. Brunger, A. T., Adams, P. D., Clore, G. M., DeLano, W. L., Gros, P., Grosse-Kunstleve, R. W., Jiang, J. S., Kuszewski, J., Nilges, M., Pannu, N. S., Read, R. J., Rice, L. M., Simonson, T., and Warren, G. L. (1998) Crystallography & NMR system: a new software suite for macromolecular structure determination. *Acta Crystallogr. D 54*, 905–921.
28. Collaborative Computational Project Number 4 (1994) The CCP4 suite: programs for protein crystallography. *Acta Crystallogr. D 50*, 760–763.
29. Emsley, P., and Cowtan, K. (2004) Coot: model-building tools for molecular graphics. *Acta Crystallogr. D 60*, 2126–2132.
30. Laskowski, R., MacArthur, M., Moss, D., and Thornton, J. (1993) PROCHECK: a program to check the stereochemical quality of protein structures. *J. Appl. Crystallogr. 26*, 283–291.
31. Hayward, S., and Berendsen, H. J. (1998) Systematic analysis of domain motions in proteins from conformational change: new results on citrate synthase and T4 lysozyme. *Proteins 30*, 144–154.
32. Seetharamappa, J., Oke, M., Liu, H., McMahon, S. A., Johnson, K. A., Carter, L., Dorward, M., Zawadzki, M., Overton, I. M., van Niekirk, C. A., Graham, S., Botting, C. H., Taylor, G. L., White, M. F., Barton, G. J., Coote, P. J., and Naismith, J. H. (2007) Expression, purification, crystallization, data collection and preliminary biochemical characterization of methicillin-resistant *Staphylococcus aureus* Sar2028, an aspartate/tyrosine/phenylalanine pyridoxal-5′-phosphate-dependent aminotransferase. *Acta Crystallogr. F 63*, 452–456.
33. Zheng, R., Dam, T. K., Brewer, C. F., and Blanchard, J. S. (2004) Active site residues in *Mycobacterium tuberculosis* pantothenate synthetase required in the formation and stabilization of the adenylate intermediate. *Biochemistry 43*, 7171–7178.
34. Ramachandran, G. N., and Sasisekharan, V. (1968) Conformation of polypeptides and proteins. *Adv. Protein Chem. 23*, 283–438.
35. Thompson, J. D., Higgins, D. G., and Gibson, T. J. (1994) CLUSTAL W: improving the sensitivity of progressive multiple sequence alignment through sequence weighting, position-specific gap penalties and weight matrix choice. *Nucleic Acids Res. 22*, 4673–4680.
36. Gouet, P., Courcelle, E., Stuart, D. I., and Metoz, F. (1999) ESPript: analysis of multiple sequence alignments in PostScript. *Bioinformatics 15*, 305–308.
37. Kabsch, W., and Sander, C. (1983) Dictionary of protein secondary structure: pattern recognition of hydrogen-bonded and geometrical features. *Biopolymers 22*, 2577–2637.
38. Wallace, A. C., Laskowski, R. A., and Thornton, J. M. (1995) LIGPLOT: a program to generate schematic diagrams of protein-ligand interactions. *Protein Eng. 8*, 127–134.